OUKA
The University of Osaka
Institutional Knowledge Archive

Title	Implantation of Human-Induced Pluripotent Stem Cell-Derived Cartilage in Bone Defects of Mice
Author(s)	Iimori, Yuki; Morioka, Miho; Koyamatsu, Saeko et al.
Citation	Tissue Engineering - Part A. 2021, 27(21-22), p. 1355-1367
Version Type	AM
URL	https://hdl.handle.net/11094/93307
rights	© Copyright 2021, Mary Ann Liebert, Inc., publishers 2021.
Note	

The University of Osaka Institutional Knowledge Archive : OUKA

https://ir.library.osaka-u.ac.jp/

The University of Osaka

Implantation of human iPS cell-derived cartilage in bone defects of mice

Yuki Iimori, M.D.[1,2], Miho Morioka, B.S.[1], Saeko Koyamatsu, M.S.[1], Noriyuki Tsumaki, M.D., Ph.D[1]

[1]Cell Induction and Regulation Field, Department of Clinical Application, Center for iPS Cell Research and Application, Kyoto University
53 Kawahara-cho, Shogoin, Sakyo-ku, Kyoto 606-8507, Japan
Tel: +81-75-366-7045, Fax: +81-75-366-7047

[2]Department of Orthopaedic Surgery, Osaka University Graduate School of Medicine
2-2 Yamadaoka, Suita 565-0871, Japan
Tel: +81-6-6879-3552, Fax: +81-6-6879-3559

E-mail address
Yuki Iimori, y.iimori@cira.kyoto-u.ac.jp
Miho Morioka, miho.morioka@cira.kyoto-u.ac.jp
Saeko Koyamatsu, s.koyamatsu@cira.kyoto-u.ac.jp
Noriyuki Tsumaki, ntsumaki@cira.kyoto-u.ac.jp

Corresponding author: Noriyuki Tsumaki

Running Head: Application of iPS cell-derived cartilage for bone defects

Keywords: induced pluripotent stem cells, cartilage, bone defect, fracture, endochondral bone formation, regeneration

Abstract

Although bone has an innate capacity for repair, clinical situations such as comminuted fracture, open fracture or the surgical resection of bone tumors produce critical-sized bone defects that exceed the capacity and require external intervention. Initiating endochondral ossification (EO) by the implantation of a cartilaginous template into the bone defect is a relatively new approach to cure critical-sized bone defects. The combination of chondrogenically primed mesenchymal stromal / stem cells and artificial scaffolds has been the most extensively studied approach for inducing endochondral bone formation in bone defects. In this study, we prepared cartilage (hiPS-Cart) from human induced pluripotent stem cells (hiPSCs) in a scaffoldless manner and implanted hiPS-Cart into 3.5 mm large defects created in the femurs of immunodeficient mice to examine the repair capacity. For the control, nothing was implanted into the defects. The implantation of hiPS-Cart significantly induced more new bone in the defect compared to the control. Culture periods for the chondrogenic differentiation of hiPSCs significantly affected the speed of the bone induction, with less time resulting in faster bone formation. Histological analysis revealed that hiPS-Cart induced new bone formation in a manner resembling EO of the secondary ossification center, with the cartilage canal, which extended from the periphery to the center of hiPS-Cart, initially forming in unmineralized cartilage, followed by chondrocyte hypertrophy at the center. In the newly formed bone, the majority of osteocytes, osteoblasts and adipocytes expressed human nuclear antigen, suggesting that these types of cells mainly derived from the perichondrium of hiPS-Cart. Osteoclasts and blood vessel cells did not express human nuclear antigen and thus were mouse. Finally, integration between the newly formed bone and mouse femur was attained substantially. Although hiPS-Cart induced new bone that filled bone defects, the

newly formed bone which is a hybrid of human and mouse had not remodeled to mature bone within the observation period of this study (28 weeks).

Impact statement

Although bone has an innate capacity for repair, critical-sized bone defects that exceed the capacity require external intervention. We prepared cartilage (hiPS-Cart) from human induced pluripotent stem cells (hiPSCs) in a scaffoldless manner and examined whether implantation of hiPS-Cart heals critical-sized defects created in the femurs of immunodeficient mice. The implantation of hiPS-Cart induced new bone in the defect in a manner resembling endochondral bone formation of the secondary ossification center. Although hiPS-Cart induced new bone that filled bone defects, the newly formed bone which is a hybrid of human and mouse had not remodeled to mature bone within the observation period of this study (28 weeks).

Introduction

Although bone has an innate capacity for repair, large-sized defects do not heal spontaneously. Comminuted fracture, open fracture or the surgical resection of bone tumors often results in critical-sized bone defects that remain unhealed and require external intervention. There are several approaches for treating critical-sized bone defects of long bones, including autologous bone graft, allogeneic bone graft, the administration of growth factors such as BMPs, and the implantation of scaffold with or without osteogenic cells. Each approach has its own strengths and weaknesses and produces mixed results(1, 2). Although autologous bone graft gives better bone formation than

allogeneic bone graft(3), it is hard to procure at sufficient amounts and is associated with donor site morbidity. Poor integration and necrosis of the bone grafts are also problematic(4, 5). As for bone allografts, a third result in failure(6).

The initiation of endochondral ossification (EO) by implantation of a cartilaginous template into the bone defect is a relatively new approach(7). Because fractures heal through an EO-like process by the initial formation of the cartilaginous callus followed by its replacement with bone callus, recapitulating the EO process during development is theoretically promising for creating new bone in bone defects and has been recently called developmental engineering(8, 9). Initially, this approach implanted cartilaginous templates into subcutaneous tissue or skull bone defects(10), but subsequent experiments using human chondrocytic cells have also confirmed new bone formation in long bone defects(8, 9, 11-15).

To initiate EO, chondrocytes and the appropriate extracellular matrix (ECM) are needed. The implantation of pellets of chondrogenically primed bone marrow-derived mesenchymal stromal / stem cells (MSCs) without scaffold resulted in limited bone formation(12). Accordingly, reports have employed an extrinsic scaffold in which chondrocytic cells are embedded to prepare the materials to be implanted into the bone defects(10). The sources of the chondrocytic cells include MSCs from bone marrow or adipose tissue and periosteal cells, because these cells have the ability to express the chondrocytic phenotype under specific chondrogenic conditions in vitro. Although the MSCs and periosteal cells has been most extensively studied as the material for EO induction in bone defects, these somatic cells lose their potential for chondrocytic differentiation after expansion. In addition, artificial scaffolds partially fail to accommodate the physiological process of EO.

The embryonic development of long bone involves two types of EO that occur serially(16, 17). Primordial cartilage undergoes the first type of EO, which gives rise to the primary ossification center (POC) at the center of the primordia, leaving epiphyseal cartilage at both ends. Then the epiphyseal cartilage postnatally undergoes the second type of EO, which brings about the secondary ossification center (SOC). Although EO that produces the POC (POC-EO) and EO that produces the SOC (SOC-EO) have much in common, histological(18) studies and recent genetic lineage tracing studies(19, 20) have revealed unique features between the two. First, while the perichondrium turns to bone collar before POC-EO occurs, the perichodrium (periarticular region) remains unmineralized in SOC-EO. Second, SOC-EO starts with the formation of cartilage canals that carry blood vessels and connective tissue into the centrally located cartilage. Third, the cartilage canals initially invade unmineralized epiphyseal cartilage during SOC-EO, whereas vessels and osteoblastic cells migrate into calcified hypertrophic cartilage during POC-EO. Previous studies on implants that initiate EO to repair bone defects reported the importance of the presence of hypertrophic chondrocytes before implantation(7, 21-25), suggesting that these implants recapitulate the POC-EC process.

Pluripotent stem cells (PSCs) such as embryonic stem cells (ESCs) and induced pluripotent stem cells (iPSCs) have both self-renewal activity and pluripotency, and thus an unlimited number of chondrocytes can be obtained by chondrogenically differentiating them in vitro. From a clinical perspective, iPSCs are sometimes preferred, because they are reprogrammed somatic cells free from the ethical issues of sacrificing embryos that are associated with ESCs. In addition, iPSCs have been established from cells from donors homozygous for major HLA loci, reducing the risk of immune rejection when the iPSC-derived differentiated cells are implanted in an allogeneic manner. Based on these

points, chondrocytes derived from iPSCs are a promising cell source for material that initiates endochondral bone formation after implantation into bone defects. However, previous studies using PSC-based material were limited to mouse ESC-derived chondrocytes seeded on a ceramic scaffold and implanted into calvarial defects(26). Taking advantage of the robust differentiating potential of human iPSCs, we have shown that cartilage can be created from human iPSC-derived chondrocytes in a scaffoldless manner by making the chondrocytes produce intrinsic cartilage ECM in suspension culture(27). In the present study, we show that the implantation of the cartilage created from human iPSCs in a scaffoldless manner (hiPS-Cart) produces new bone in critical-sized bone defects in the femur of SCID mice through a process that is reminiscent of SOC-EO.

Materials and Methods

Ethics statement

All methods were carried out in accordance with relevant guidelines and regulations. Experiments using recombinant DNA were approved by the Recombinant DNA Experiments Safety Committee of Kyoto University. Research involving human subjects was approved by the Ethics Committee of Kyoto University. Written informed consent was obtained from the donor. All animal experiments were approved by the institutional animal committee of Kyoto University.

iPSCs and creation of scaffoldless hiPS-Cart

The hiPSC line QHJI was generated from a healthy individual who is homozygous for major HLA loci and was a gift from K. Okita, M. Nakagawa, and S. Yamanaka (Center for iPS Cell Research and Application (CiRA), Kyoto University, Kyoto, Japan). QHJI was generated from reprogramming human peripheral mononuclear cells by electroporating into them episomal plasmid vectors (pCXLE-hOCT3/4-shp53-F, hSK, hUL, EBNA)(28). All cells were negative for genome integration of the vector sequences.

For the creation of hiPS-Cart, the hiPSCs were chondrogenically differentiated following a previously described method(27) with modification. hiPS-Cart were created by cultivating hiPSCs in chondrogenic medium (DMEM (Sigma) with 1% ITS, 1% FBS (Thermo), 1 x 10^{-4} M nonessential amino acids (Thermo), 1 mM Na pyruvate (Thermo), 50 units of penicillin, 50 mg/ml of streptomycin, 50 μg/ml ascorbic acid (Nacalai), 10 ng/ml BMP2 (Peprotech), 10 ng/ml TGFβ1 (Peprotech) and 10 ng/ml GDF5 (PTT))(27) for 10, 12 and 17 weeks.

Real-time RT-PCR analysis

hiPSC-derived particles were homogenized using a multi beads shocker (Yasui kikai). Total RNA was isolated using QIAzol (Qiagen) and RNeasy Mini Kits (Qiagen) with the RNase-Free DNase Set (Qiagen) according to the manufacturer's instructions. A total of 400 ng RNA was used as the template for the cDNA synthesis using ReverTra

Ace (TOYOBO). Real-time PCR was performed in a Step One system (ABI) using a KAPA SYBR FAST qPCR kit Master Mix ABI prism (KAPA BIOSYSTEMS). The primers used are listed in Table 1.The amplified products were used to derive standard curves for quantitative real-time PCR. The mRNA expression levels were normalized to the level of the *GAPDH* expression.

Implantation of hiPS-Cart into femoral defects created in SCID mice

Male 10-week-old CB-17/Icr-scid/scidJcl (SCID) mice (CLEA Japan, Tokyo, Japan) were anesthetized. The left femur was exposed through the lateral approach. After fixing a metal plate (RISystem Mouse Fix) onto the femur, a defect of 3.5 mm was created with a Gigli wire saw. hiPS-Cart was put into the defect and fixed to the metal plate with a 5-0 nylon thread. For the control group, the defect was made but left empty. Mice were periodically anesthetized, and their left femur was subjected to X-ray analysis. At the time of sacrifice, carbon dioxide was administrated to the mice. After taking X-ray images of the left femur, the femur was harvested from each animal and serially subjected to micro-CT imaging and histological analysis.

X-ray analysis

The lateral view of the left femur was taken using an X-ray imaging device (Model DX-50, Faxitron Bioptics, AZ, USA) at 26 kV, 0.1 mA. The longitudinal lengths of the newly formed bones in the defects were measured with ImageJ software (National Institutes of Health). The bone extending from the femur was not included in the measurement of newly formed bone, because it was also observed in the control group.

Micro-CT analysis

Femurs were subjected to a micro-CT imaging system (inspeXio SMX-100CT, Shimadzu, Kyoto, Japan) at 60 kV, 200 μA and 50 μm/voxel with a metal filter. The tissue volume of the newly formed bone in the defects was measured using TRI 3D/BON software (RATOC system engineering, Tokyo, Japan).

Histological analysis

The femurs were fixed in 4% paraformaldehyde for 4 days, decalcified in 10% ethylenediaminetetraacetic acid for 14 days, and embedded in paraffin. Semi-serial sections were prepared and stained with hematoxylin and eosin (HE) or Safranin O-fast green-iron hematoxylin (Safranin O) or were immunostained with specific antibodies. The primary antibodies used are listed in Table 2 and were detected with a CSA II Biotin-free Tyamide Signal Amplification System Kit (Agilent Technologies, CA, USA) and DAB as a chromogen. TRAP staining was performed using the TRAP Staining Kit (COSMO Bio Co., LTD). Picrosirius red staining was performed using the Picrosirius Red Stain Kit (COSMO Bio Co., LTD). Safranin O-positive areas were measured using a BZ analyzer II (KEYENCE).

Statistical analysis

The data are shown as averages and 95% Confidence Intervals. In this study, we used Tukey's multiple comparisons test. p-Values < 0.05 were considered statistically significant.

Results

Implantation of hiPS-Cart produced new bone in critical-sized defects in femur.

We created hiPS-Cart, which are cartilaginous particles, by chondrogenically differentiating hiPSCs toward chondrocytes, followed by transfer into three-dimensional culture to make the chondrocytes produce ECM by themselves (Fig. 1A). To evaluate whether the cultivation period for the chondrogenic differentiation affects bone formation capacity, we prepared hiPS-Cart with different cultivation periods (10 weeks, 12 weeks or 17 weeks; designated as hiPS-Cart-10w, hiPS-Cart-12w or hiPS-Cart-17w, respectively) for the chondrogenic differentiation. Histological analysis confirmed that hiPS-Cart consisted of cartilage expressing type II collagen (COL2) at the center wrapped by perichondrium expressing type I collagen (COL1)-like primordial cartilage (Fig. 1B). Real-time RT-PCR analysis revealed that hiPS-Cart highly expressed *COL2A1* and *ACAN* genes, which respectively encode the cartilage ECM proteins type II collagen α1 chain and aggrecan, in all hiPS-Cart compared with hiPSCs (Fig. 1C). The mRNA expression levels of type X collagen gene (*COL10A1)*, a marker for the zone of hypertrophic chondrocytes, were constantly low throughout the chondrogenic differentiation period and did not differ much from the level in hiPSCs (Fig.1C). The expression of type X collagen (COL10) was also low at the protein level (Fig. 1B).

We implanted these hiPS-Carts into 3.5 mm defects created in the middle of the femoral shafts (each group N = 5 mice) (Fig. 1D). As a control, we left the defect empty (N = 6 mice). We took X-ray images at 4, 8, 16 and 28 weeks after the implantation under anesthesia to measure the sizes of the newly formed bone. One mouse that received hiPS-Cart-10w, one mouse that received hiPS-Cart-12w and one mouse that received hiPS-Cart-17w respectively died at 8, 24 and 20 weeks after the implantation. All three died

after anesthesia, which appeared to be the cause of their deaths. At 28 weeks after the implantation, we sacrificed the other mice and dissected the femur for micro-CT analysis.

The implantation of hiPS-Cart-10w caused an earlier formation of new bones of bigger size than the implantation of hiPS-Cart-12w or hiPS-Cart-17w at each period examined (Fig. 2A,B). There was no new bone formation at 4 weeks after implantation, but at 8 weeks after, a substantial amount of bone was formed in sites in which hiPS-Cart-10w was implanted. At the same time, small ossification or calcification was recognized at sites in which hiPS-Cart-12w was implanted, and no bone formation at sites in which hiPS-Cart-17w was implanted. The sizes of the newly formed bone increased gradually at 16 and 28 weeks after the implantation.

Micro CT analysis also revealed that the tissue volume of newly formed bone created by the implantation of hiPS-Cart-10w was larger than that of hiPS-Cart-12w or hiPS-Cart-17w at 28 weeks after implantation (Fig. 2C,D). In the control group, there was no new bone formation at all observed times (Fig. 2). These results indicate that the implantation of hiPS-Cart into critical-sized bone defects in the femur of SCID mice facilitates bone healing and that the cultivation period of hiPS-Cart affects the bone formation capacity.

After the micro CT analysis, we subjected the femur to histological analysis. Safranin O staining of histological sections revealed more cartilage remnant in the samples collected after the transplantation of hiPS-Cart-12w and hiPS-Cart-17w than hiPS-Cart-10w, although the differences were not significant (Fig. 2E,F). Regarding safety, there was no obvious tumor formation in the left thigh throughout the experiments. Furthermore, histological analysis revealed no atypical nuclei indicative of malignant transformation or teratoma.

hiPS-Cart forms new bone reminiscent of the SOC-EO process.

To get insight into the biology of the bone formation after the implantation of hiPS-Cart, we implanted hiPS-Cart-10w and hiPS-Cart-17w into a new group of mice. We sacrificed them at 4, 8 and 16 weeks (for hiPS-Cart-10w) and 4, 8, 16 and 28 weeks (for hiPS-Cart-17w) after the implantation, dissected the femurs, and subjected them to X-ray, micro-CT and histological analysis.

Again, X-ray and micro-CT analysis revealed that the implantation of hiPS-Cart-10w caused faster bone formation than hiPS-Cart-17w did (Fig. 3). Although the speeds of the new bone formation were different, histological analysis revealed that the bone formation process was similar between the two conditions (Fig. 3B). The initial change found in the histological section was formation of a cord-like structure in hiPS-Cart. At four weeks after the implantation of hiPS-Cart-10w, there was no calcification at the implanted sites, as indicated by radiolucency in the micro-CT images (Fig. 4A, top row). The histological section corresponding to the micro-CT image revealed that the cord-like structure expressed COL1 and was formed in cartilaginous hiPS-Cart that expressed COL2 (Fig. 4A, second and third rows). There was no expression of COL10 (Fig. 4A, second and third rows). The cord-like structure extended from the COL1-positive perichondrium of hiPS-Cart to the center of the unmineralized and un-hypertrophic hiPS-Cart (Fig. 4A, second and third rows). Higher magnification revealed that the cord-like structure was composed of blood vessels and connective tissue (Fig. 4A, bottom row), resembling the cartilage canal seen in the SOC-EC process.

In a sample harvested four weeks after the implantation of hiPS-Cart-17w, chondrocytes near the cord-like structure in the center of hiPS-Cart appeared to begin

hypertrophy, as indicated by the COL10 expression (Fig. 4C). These changes were followed by bone formation beginning from the center of hiPS-Cart, as indicated by the histology and micro-CT images of samples harvested at later stages (Fig. 3B). This sequence of events is characteristic of SOC-EO, but not of POC-EO, suggesting that hiPS-Cart formed bone in a manner resembling the SOC-EO process.

Newly formed bone is composed of both human and mouse cells.

Immunohistochemical analysis at 4 weeks after implantation using an antibody that recognizes human nuclear antigen (HNA) revealed that the nuclei of fibrous cells in the connective tissue in the cartilage canal were mainly HNA-positive, but that cells composing blood vessels and marked with CD31 were HNA-negative (Fig. 4A, bottom row, and Fig. 4B). These results suggest that the fibrous cells were derived from hiPS-Cart and mouse, while cells composing blood vessels were derived from mouse only.

We recognized adipocytes in the bone marrow in the newly formed bone at 16 weeks after the implantation (Fig. 5A, top and middle rows). The majority of adipocytes, but not all, were HNA-positive (Fig. 5A, yellow arrows in the middle row, and Fig. 5B), suggesting that the adipocytes were derived from hiPS-Cart and mouse. Cells embedded in the bony matrix were mostly HNA-positive (Fig. 5A, green arrowheads in the middle row, and Fig. 5B), suggesting that most osteocytes were derived from hiPS-Cart. Among cells on the surface of the bony matrix, the majority were HNA-positive (Fig. 5A, red arrows in the middle row, and Fig. 5B), suggesting that osteoblasts were derived from hiPS-Cart and mouse. We also recognized multinucleated TRAP-positive cells, all of which were HNA-negative (Fig. 5A, blue arrowheads in the bottom row, and Fig. 5B), suggesting that osteoclasts were derived from mouse only.

Apart from the newly formed bone in the center of hiPS-Cart through a SOC-EO-

like process, another bone type was formed around the periphery of hiPS-Cart. Micro-CT images revealed a thin shell-like layer of ossification wrapping around part of hiPS-Cart (Fig. 6A, top row, and Fig. 6B). The calcified bony matrix was COL1-positive and COL10-negative (Fig. 6A, middle row), indicating that hypertrophic chondrocytes were not present. Most of the osteocytes and osteoblasts were HNA-positive, and all of the osteoclasts were HNA-negative (Fig. 6A, bottom row, and Fig. 6C). These results collectively suggest that this bone was directly formed from the perichondrium of hiPS-Cart as bone collar through the membranous ossification process.

Newly formed bone from hiPS-Cart integrated with native femoral bone.

Micro-CT analysis and histological analysis also revealed the continuity between newly formed bone and mouse native femoral bone (Fig. 7, top row). Bony matrix expressed COL1 (Fig. 7, middle row) and could be divided into two areas: one area that contained HNA-positive osteocytes, and one area that contained HNA-negative osteocytes (Fig 7, right panel in middle row). These results indicate that the newly formed bone from hiPS-Cart contacted the mouse femoral bone. Picrosirius red staining revealed some accordance in the direction of collagen fibrils between the newly formed bone and mouse bone (Figure 7, bottom row), suggesting the occurrence of bone union between the newly formed bone from hiPS-Cart and mouse native femoral bone.

Discussion

This study demonstrated that cartilage generated from human iPSCs can create new bone in defects in long bone in the absence of artificial scaffold. hiPS-Cart consists of chondrocytes embedded in cartilaginous ECM produced by hiPS-Cart chondrocytes. We propose that the dispensability of extrinsic scaffold is owed to the ability of hiPSC-derived chondrocytes to produce abundant cartilage ECM, as evidenced by the intense staining of hiPS-Cart with Safranin O (Fig. 1B).

We previously reported that hiPS-Cart forms embryonic skeleton composed of the POC and epiphyseal cartilage after implantation into the subcutaneous spaces of SCID mice(29), suggesting that hiPS-Cart initiates POC-EO there. On the other hand, the present study showed that hiPS-Cart initiated a SOC-EO-like process after implantation into femoral bone defects, suggesting that the environment affects the mode of EO. The environmental factors that determine whether POC-EO or SOC-EO is initiated remain to be analyzed.

Tong et al. closely analyzed SOC-EO using lineage tracing technology, finding that osteoblasts, osteocytes and adipocytes in the SOC are derived from the perichondrium, from which the cartilage canal initiates(20). Accordingly, our results, in which most osteoblasts, osteocytes and adipocytes in the newly formed bone were human, suggest that the osteogenic cells were derived from perichondrial cells in hiPS-Cart. That blood vessels and osteoclasts were derived from mouse supports the absence of endothelial cells or hematopoietic cells in hiPS-Cart.

During SOC-EO, cartilage canals start to form at several sites in the perichondrium, but how these locations are specified is not known. In the present study, the canals extended from the perichondrium of hiPS-Cart at the sites that contacted the margins of

the femur of the host, suggesting unknown factors from the host bone activate a segment in the perichondrium of hiPS-Cart to initiate canal formation.

Although it has been reported that ectopic bone formation depends on the presence of hypertrophic chondrocytes in the implants(7, 21-25), SOC-EO starts in the absence of hypertrophic chondrocytes(18, 20), thus, ectopic bone should form irrespective of the presence or absence of hypertrophic chondrocytes. Our results showing that a shorter culture period of hiPS-Cart caused quicker ossification in long defects and was not associated with increased COL10 expression are consistent with the conclusion that hiPS-Cart underwent a SOC-EO-like process in the long bone defects. Thyroid hormone(30), epidermal growth factor receptor (EGFR)(31), Wnt/β-catenin(32) and insulin-like growth factor(33) are all reported to regulate the occurrence of SOC-EO. It remains to be analyzed whether these or other signals are involved in the ossification of hiPS-Cart after implantation into bone defects.

Although hiPS-Cart induced new bone that filled bone defects, the newly formed bone had not remodeled to mature bone within the observation period of this study (28 weeks). It is difficult to evaluate the rate of maturation, because the new bone is a hybrid of human and mouse, since it is produced by human osteoblasts/osteocytes and mouse osteoblasts/osteocytes, and human bone matures much more slowly than mouse bone. Longer observation will be needed to confirm the maturation of newly formed bone from hiPS-Cart in future studies using primate models. In addition, the inclusion of a positive control, such as BMP2 treatment, will provide insight on the rates and quality of bone healing brought by hiPS-Cart transplantation.

Additionally, we estimate the scalability of hiPS-Cart to be enough to fill bone defects in human. We base this conclusion on having subjected 1.5 x 10^6 iPSCs to

chondrogenic differentiation in ten 10 cm dishes from which we obtained 250 hiPS-Cart particles, or about 10 g in total. The amount of hiPS-Cart needed to fill bone defects in human can reach around 10 cm^3, which is 10 g or more. However, iPSCs can be expanded unlimitedly and the culture is scalable by increasing the number of dishes.

hiPSCs can be created from patients, enabling the autografting of hiPSC-derived cells. However, it takes time and is costly to prepare autologous hiPSCs. The use of allogeneic iPSCs can be one solution but risks immune rejection. To overcome this issue, a bank of allogenic clinical GMP cell lines are being established(28, 34). This iPSC bank will be prepared from donors who are homozygous for major HLA types. With regards to clinical settings, an iPSC line with the HLA type that matches the patient's will be selected, subjected to chondrogenic differentiation and used for the implantation. It is estimated that a bank of 100 cell lines homozygous for major HLA types could match the majority of the world population(28, 35). The QHJI hiPSC line we used in this study was generated from the blood cells of a healthy donor who is homozygous for the most common HLA type in Japan(36) and matches 17% of the Japanese population at three major loci. Thus, QHJI hiPS-Cart could be applicable to allogeneic implantation for this population, although further immunogenic studies are needed before clinical application.

When using MSCs as the cell source, the bone regeneration is donor-dependent, because the differentiating potential of MSCs between individuals varies(13). Therefore, the preparation of chondrogenically differentiated MSCs for each single donor needs to be established before the application, making this approach difficult for translation to clinical settings. On the other hand, HLA-homo iPSCs have self-renewal activity and can be expanded almost infinitely. Therefore, uniform hiPS-Cart from a single donor can be provided for a large number of patients.

The use of hiPSCs has several issues that must be overcome before their clinical application. Because the creation of iPSCs requires a reprogramming process that is absent in the preparation of MSCs, the tumorigenic risks associated with iPSCs are higher than those with MSCs. Three mice died in the middle of our experiments after the implantation of hiPS-Cart, but these deaths were attributed to the anesthesia performed during taking X-ray images. There was no obvious tumor formation throughout the experiments, although longer observation periods are needed to prove safety. Furthermore, our results indicated that a shorter culture period resulted in quicker bone formation after implantation, however, the shorter period also increases the risk of contaminating undifferentiated cells that could give rise to teratoma after implantation. Therefore, the safety of hiPS-Cart needs to be cautiously examined before its translation to clinical settings.

Acknowledgements

We thank Tomoko Kato for the histological analysis, Masumi Sanada for the analysis of hiPS-Cart, and Hiromi Nishino, Makiko Matsuoka, Fumiko Hamada, Aoi Okamoto, Hiroko Nakagawa and Chie Ota for the preparation of hiPS-Cart. We thank Peter Karagiannis for reading the manuscript, and Akihiro Yamashita, Kaori Fujita, Nobuyuki Shima and Nanao Horike for discussions.

Funding: This study was supported by Scientific Research Grant No. 18H02923 (to N.T.) from the Ministry of Education, Culture, Sports, Science and Technology (MEXT), Japan, and the Practical Research Project for Rare / Intractable Diseases (step 1) Grant No. 20ek0109452h0001 (to N.T.), Centers for Clinical Application Research on Specific Disease/Organ (type B) Grant No. 17bm0304004h0005 (to N.T.), Research Project for Practical Applications of Regenerative Medicine Grant No. 19bk0104079h0001 (to N. T.),

Core Center for iPS Cell Research Grant No. 17bm0104001h0005 (to N.T.), and the Acceleration Program for Intractable Diseases Research utilizing Disease-specific iPS cells Grant No. 17bm0804006h0001 (to N.T.) from the Japan Agency for Medical Research and Development (AMED).

Author contributions

Y.I. and N.T. designed the study. M.M. and S.K. prepared and analyzed hiPS-Cart. Y.I. implanted hiPS-Cart into mice and analyzed the samples. Y.I. and N.T. wrote the manuscript. N.T. conceived the study.

Data availability

All original data including real-time RT-PCR, X-ray, micro-CT and histological data are available upon request to the authors.

References

1. Amini, A.R., Laurencin, C.T., and Nukavarapu, S.P. Bone tissue engineering: Recent advances and challenges. Crit Rev Biomed Eng **40**, 363, 2012.

2. Salgado, A.J., Coutinho, O.P., and Reis, R.L. Bone tissue engineering: State of the art and future trends. Macromolecular Bioscience **4**, 743, 2004.

3. Flierl, M.A., Smith, W.R., Mauffrey, C., et al. Outcomes and complication rates of different bone grafting modalities in long bone fracture nonunions: a retrospective cohort study in 182 patients. Journal of orthopaedic surgery and research **8**, 33, 2013.

4. Nguyen, L.H., Annabi, N., Nikkhah, M., et al. Vascularized bone tissue engineering: approaches for potential improvement. Tissue engineering Part B, Reviews **18**, 363, 2012.

5. Bauer, T.W., and Muschler, G.F. Bone graft materials. An overview of the basic science. Clin Orthop Relat Res, 10, 2000.

6. Brigman, B.E., Hornicek, F.J., Gebhardt, M.C., and Mankin, H.J. Allografts about the Knee in Young Patients with High-Grade Sarcoma. Clin Orthop Relat Res, 232, 2004.

7. Scotti, C., Tonnarelli, B., Papadimitropoulos, A., et al. Recapitulation of endochondral bone formation using human adult mesenchymal stem cells as a paradigm for developmental engineering. Proc Natl Acad Sci U S A **107**, 7251, 2010.

8. McDermott, A.M., Herberg, S., Mason, D.E., et al. Recapitulating bone development through engineered mesenchymal condensations and mechanical cues for tissue regeneration. Sci Transl Med **11**2019.

9. Nilsson Hall, G., Mendes, L.F., Gklava, C., Geris, L., Luyten, F.P., and Papantoniou, I. Developmentally Engineered Callus Organoid Bioassemblies Exhibit Predictive In Vivo Long Bone Healing. Advanced science (Weinheim, Baden-Wurttemberg, Germany) **7**, 1902295, 2020.

10. Dennis, S.C., Berkland, C.J., Bonewald, L.F., and Detamore, M.S. Endochondral ossification for enhancing bone regeneration: converging native extracellular matrix biomaterials and developmental engineering in vivo. Tissue engineering Part B, Reviews **21**, 247, 2015.

11. Bernhard, J., Ferguson, J., Rieder, B., et al. Tissue-engineered hypertrophic chondrocyte grafts enhanced long bone repair. Biomaterials **139**, 202, 2017.

12. Bahney, C.S., Hu, D.P., Taylor, A.J., et al. Stem cell-derived endochondral cartilage stimulates bone healing by tissue transformation. J Bone Miner Res **29**, 1269, 2014.

13. van der Stok, J., Koolen, M.K., Jahr, H., et al. Chondrogenically differentiated mesenchymal stromal cell pellets stimulate endochondral bone regeneration in critical-sized bone defects. Eur Cell Mater **27**, 137, 2014.

14. Shoji, T., Ii, M., Mifune, Y., et al. Local transplantation of human multipotent adipose-

derived stem cells accelerates fracture healing via enhanced osteogenesis and angiogenesis. Lab Invest **90**, 637, 2010.

15. Bahney, C.S., Jacobs, L., Tamai, R., et al. Promoting Endochondral Bone Repair Using Human Osteoarthritic Articular Chondrocytes. Tissue Eng Part A **22**, 427, 2016.

16. Kronenberg, H.M. Developmental regulation of the growth plate. Nature **423**, 332, 2003.

17. Long, F., and Ornitz, D.M. Development of the endochondral skeleton. Cold Spring Harbor perspectives in biology **5**, a008334, 2013.

18. Blumer, M.J., Longato, S., and Fritsch, H. Structure, formation and role of cartilage canals in the developing bone. Ann Anat **190**, 305, 2008.

19. Maes, C., Kobayashi, T., Selig, M.K., et al. Osteoblast precursors, but not mature osteoblasts, move into developing and fractured bones along with invading blood vessels. Dev Cell **19**, 329, 2010.

20. Tong, W., Tower, R.J., Chen, C., et al. Periarticular Mesenchymal Progenitors Initiate and Contribute to Secondary Ossification Center Formation During Mouse Long Bone Development. Stem Cells **37**, 677, 2019.

21. Scotti, C., Piccinini, E., Takizawa, H., et al. Engineering of a functional bone organ through endochondral ossification. Proc Natl Acad Sci U S A **110**, 3997, 2013.

22. Sheehy, E.J., Vinardell, T., Toner, M.E., Buckley, C.T., and Kelly, D.J. Altering the architecture of tissue engineered hypertrophic cartilaginous grafts facilitates vascularisation and accelerates mineralisation. PLoS ONE **9**, e90716, 2014.

23. Oliveira, S.M., Mijares, D.Q., Turner, G., Amaral, I.F., Barbosa, M.A., and Teixeira, C.C. Engineering endochondral bone: in vivo studies. Tissue Eng Part A **15**, 635, 2009.

24. Oliveira, S.M., Amaral, I.F., Barbosa, M.A., and Teixeira, C.C. Engineering endochondral bone: in vitro studies. Tissue Eng Part A **15**, 625, 2009.

25. Vinardell, T., Sheehy, E.J., Buckley, C.T., and Kelly, D.J. A comparison of the functionality and in vivo phenotypic stability of cartilaginous tissues engineered from different stem cell sources. Tissue Eng Part A **18**, 1161, 2012.

26. Jukes, J.M., Both, S.K., Leusink, A., Sterk, L.M., van Blitterswijk, C.A., and de Boer, J. Endochondral bone tissue engineering using embryonic stem cells. Proc Natl Acad Sci U S A **105**, 6840, 2008.

27. Yamashita, A., Morioka, M., Yahara, Y., et al. Generation of Scaffoldless Hyaline Cartilaginous Tissue from Human iPSCs. Stem cell reports **4**, 404, 2015.

28. Okita, K., Matsumura, Y., Sato, Y., et al. A more efficient method to generate integration-free human iPS cells. Nat Meth **8**, 409, 2011.

29. Kimura, T., Ozaki, T., Fujita, K., et al. Proposal of patient-specific growth plate cartilage xenograft model for FGFR3 chondrodysplasia. Osteoarthritis Cartilage **26**, 1551, 2018.

30. Xing, W., Cheng, S., Wergedal, J., and Mohan, S. Epiphyseal chondrocyte secondary ossification centers require thyroid hormone activation of Indian hedgehog and osterix signaling. J Bone Miner Res **29**, 2262, 2014.
31. Zhang, X., Zhu, J., Li, Y., et al. Epidermal growth factor receptor (EGFR) signaling regulates epiphyseal cartilage development through β-catenin-dependent and -independent pathways. J Biol Chem **288**, 32229, 2013.
32. Dao, D.Y., Jonason, J.H., Zhang, Y., et al. Cartilage-specific β-catenin signaling regulates chondrocyte maturation, generation of ossification centers, and perichondrial bone formation during skeletal development. J Bone Miner Res **27**, 1680, 2012.
33. Wang, Y., Menendez, A., Fong, C., et al. IGF-I Signaling in Osterix-Expressing Cells Regulates Secondary Ossification Center Formation, Growth Plate Maturation, and Metaphyseal Formation During Postnatal Bone Development. J Bone Miner Res **30**, 2239, 2015.
34. Turner, M., Leslie, S., Martin, N.G., et al. Toward the development of a global induced pluripotent stem cell library. Cell stem cell **13**, 382, 2013.
35. Gourraud, P.-A., Gilson, L., Girard, M., and Peschanski, M. The Role of Human Leukocyte Antigen Matching in the Development of Multiethnic "Haplobank" of Induced Pluripotent Stem Cell Lines. Stem Cells **30**, 180, 2012.
36. Hanatani, T., and Takasu, N. Present and Future of an iPS Cell Stock for Regenerative Medicine. Rinsho Byori **65**, 160, 2017.

Implantation of human iPS cell-derived cartilage in bone defects of mice

Yuki Iimori[1,2], Miho Morioka[1], Saeko Koyamatsu[1], Noriyuki Tsumaki[1]

[1]Cell Induction and Regulation Field, Department of Clinical Application, Center for iPS Cell Research and Application, Kyoto University, Japan

[2]Department of Orthopaedic Surgery, Osaka University Graduate School of Medicine, Suita, Osaka, Japan

Figure legends

Figure 1. Characterization of hiPS-Cart and its implantation into bone defects in the femur.

(A) Appearance of 3 hiPS-Cart. Scale bar, 5 mm.

(B) Semi-serial histological sections of hiPS-Cart were stained with Safranin O or immunostained with antibodies that recognize the indicated proteins. As a control for the immunohistochemical staining, staining of the semi-serial sections of the proximal tibia of mouse 7 days after birth is shown in the bottom panels. Scale bars: 100 μm.

(C) Real-time RT-PCR expression analysis of chondrocytic markers in hiPS-Cart cultured for different periods. Data are presented with 95% C.I. error bars (n = 4). *P < 0.05, **P < 0.01, ***P < 0.001 and ****P < 0.0001 by Tukey's multiple comparisons test.

(D) Implantation of hiPS-Cart. After fixing a metal plate onto the femur, a defect of 3.5 mm was created. hiPS-Cart (*top row*) or nothing (*bottom row*) was implanted into the

defect and fixed to the metal plate with 5-0 nylon thread. *Left*, images after implantation. *Middle*, femur, metal plate, and screws are indicated by yellow lines. The images are otherwise the same as those on the left. *Right*, X-ray images immediately after the surgery, lateral view. Scale bars, 1 mm. All images were taken immediately after the surgery.

Figure 2. New bone formation after implantation of hiPS-Cart into femoral bone defects.

(A) X-ray images of a femur at the indicated periods after implantation (Post Op). Lateral view.

(B) Length of newly formed bones in the X-ray images. Each circle denotes one mouse.

(C) Three-dimensional reconstructed micro-CT images of the femur at 28 weeks after implantation. Newly formed bones are indicated as yellow. Lateral view.

(D) Tissue volume of the newly formed bone in the micro-CT images. Each circle denotes one mouse.

(E) Histological sections of femur at 28 weeks were stained with Safranin O.

(F) Safranin O-positive areas in (E) were measured.

Data are presented with 95% C.I. error bars. *P < 0.05, **P < 0.01, ***P < 0.001 and ****P < 0.0001 by Tukey's multiple comparisons test. Scale bars, 1 mm.

Figure 3. Micro-CT and histological analysis of newly formed bone at 4, 8 and 16 weeks (for hiPS-Cart-10w) and 4, 8, 16 and 28 weeks (for hiPS-Cart-17w) after implantation.

(A) Length in X-ray images and tissue volume in micro-CT images of newly formed bone. Each circle denotes one mouse. Data are presented with 95% C.I. error bars. *P < 0.05 and ***P < 0.001 by Tukey's multiple comparisons test.

(B) Three-dimensional reconstructed micro-CT images, two-dimensional micro-CT images and corresponding hematoxylin-eosin (HE) stained histological sections of the implanted sites are shown. #1 and #2 indicate different mice. Scale bars, 1 mm.

Figure 4. Histological analysis of implanted sites harvested four weeks after implantation of hiPS-Cart-10w (A,B) and hiPS-Cart-17w (C).

(A) *Top row*, A three-dimensional reconstructed micro-CT image (lateral view) and two-dimensional micro-CT image (sagittal) are shown. *Second row*, Semi-serial histological sections corresponding to the micro-CT image in the top row were stained with hematoxylin-eosin (HE) or immunostained with antibodies that recognize the indicated proteins. Magnifications of the blue-boxed regions are shown in the *third row*. Magnification of the green-boxed region in the left panel in the second row is shown in the *bottom row*, in which immunostained semi-serial sections are also included. HNA, human nuclear antigen.

(B) Percentage of HNA-positive cells per total cells in a field of view in the cartilage canal. *vEC*, vascular endothelial cell. *FC*, fibrous cell. Each dot denotes one field of view. Data are presented with 95% C.I. error bars.

(C) *Top row*, A three-dimensional reconstructed micro-CT image (lateral view), two-dimensional micro-CT image (sagittal) and semi-serial histological sections corresponding to the micro-CT images stained with hematoxylin-eosin (HE) or immunostained with antibodies that recognize COL10. *Bottom row*, Magnifications of the boxed regions, respectively.

Scale bars, 100 μm.

Figure 5. Origin of cells composing new bone formed through a SOC-EO-like process.

(A) *Top row*, A three-dimensional reconstructed micro-CT image (frontal view), two-dimensional micro-CT image (coronal) and corresponding hematoxylin-eosin (HE) stained histological section (coronal) of newly formed bone 16 weeks after the implantation of hiPS-Cart-17w. The magnified image of the blue-boxed region is shown in the *second row* and that of the green-colored box in the *third row*. Semi-serial histological sections were immunostained with antibodies that recognize human nuclear antigen (HNA) or TRAP. Scale bars 100 μm.

(B) Percentage of HNA-positive cells per total cells in a field of view in newly formed bone. Each dot denotes one field of view. Data are presented with 95% C.I. error bars.

Figure 6. Membranous ossification at the periphery of hiPS-Cart.

(A) *Top row*, A three-dimensional reconstructed micro-CT image (lateral view), two-dimensional micro-CT image (sagittal) and corresponding hematoxylin-eosin (HE) stained histological section (sagittal) of newly formed bone at 16 weeks after the implantation of hiPS-Cart-17w are shown. The magnified images of the boxed regions in the top and second rows are shown in the *second and bottom rows*, respectively. Semi-serial histological sections were immunostained with antibodies that recognize COL1, COL10 or human nuclear antigen (HNA) or stained with TRAP.

(B) A two-dimensional micro-CT image (axial) at the position indicated by the red lines in (A).

(C) Percentage of HNA-positive cells per total cells in a field of view in newly formed bone. Each dot denotes one field of view. Data are presented with 95% C.I. error bars.

Scale bars 100 μm.

Figure 7. Union of newly formed bone and mouse bone.

Top row, A three-dimensional reconstructed micro-CT image (lateral view), two-dimensional micro-CT image (sagittal) and corresponding hematoxylin-eosin (HE) stained histological section (sagittal) of newly formed bone at 16 weeks after the implantation of hiPS-Cart-10w. The magnified images of the blue-boxed regions in the histological section are shown in the *middle row*. Semi-serial histological sections were immunostained with antibodies that recognize COL1 or human nuclear antigen (HNA). In the right panel in the second row, the solid red lines denote the edge of bony matrix. We arbitrarily drew the red dotted line to indicate the border between the HNA-positive area and HNA-negative area. *Bottom row*, A semi-serial section was stained with picrosirius red and analyzed by polarized microscopy. The red-boxed region corresponds to the blue-boxed region above. Its magnification is shown to the right. Scale bars 100 μm.

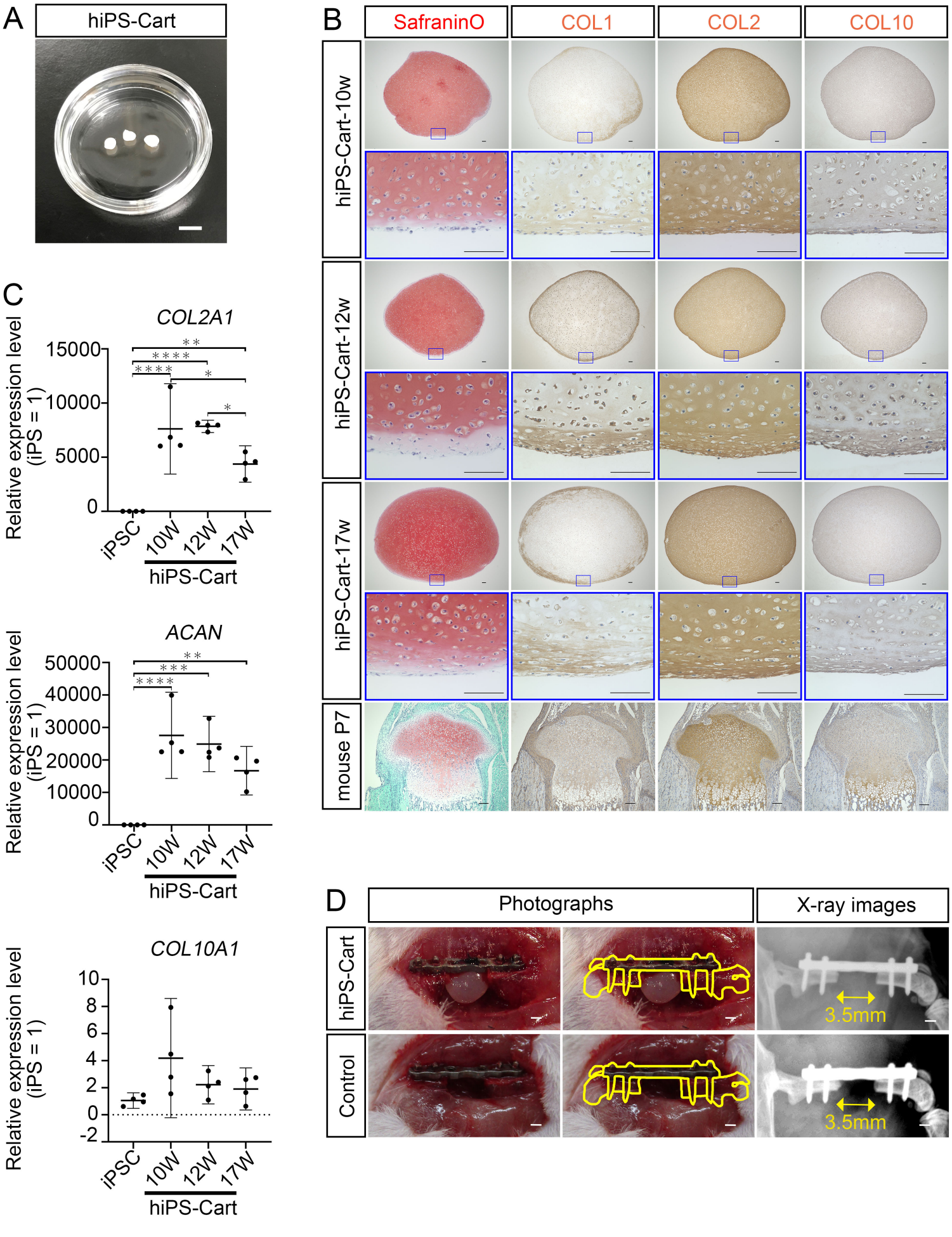
A
hiPS-Cart
B
SafraninO
COL1
COL2
COL10
hiPS-Cart-10w
hiPS-Cart-12w
hiPS-Cart-17w
mouse P7
C
COL2A1
Relative expression level (iPS = 1)
15000
10000
5000
0
iPSC
10W
12W
17W
hiPS-Cart
ACAN
50000
40000
30000
20000
10000
0
COL10A1
10
8
6
4
2
0
-2
D
Photographs
X-ray images
hiPS-Cart
Control
3.5mm
3.5mm

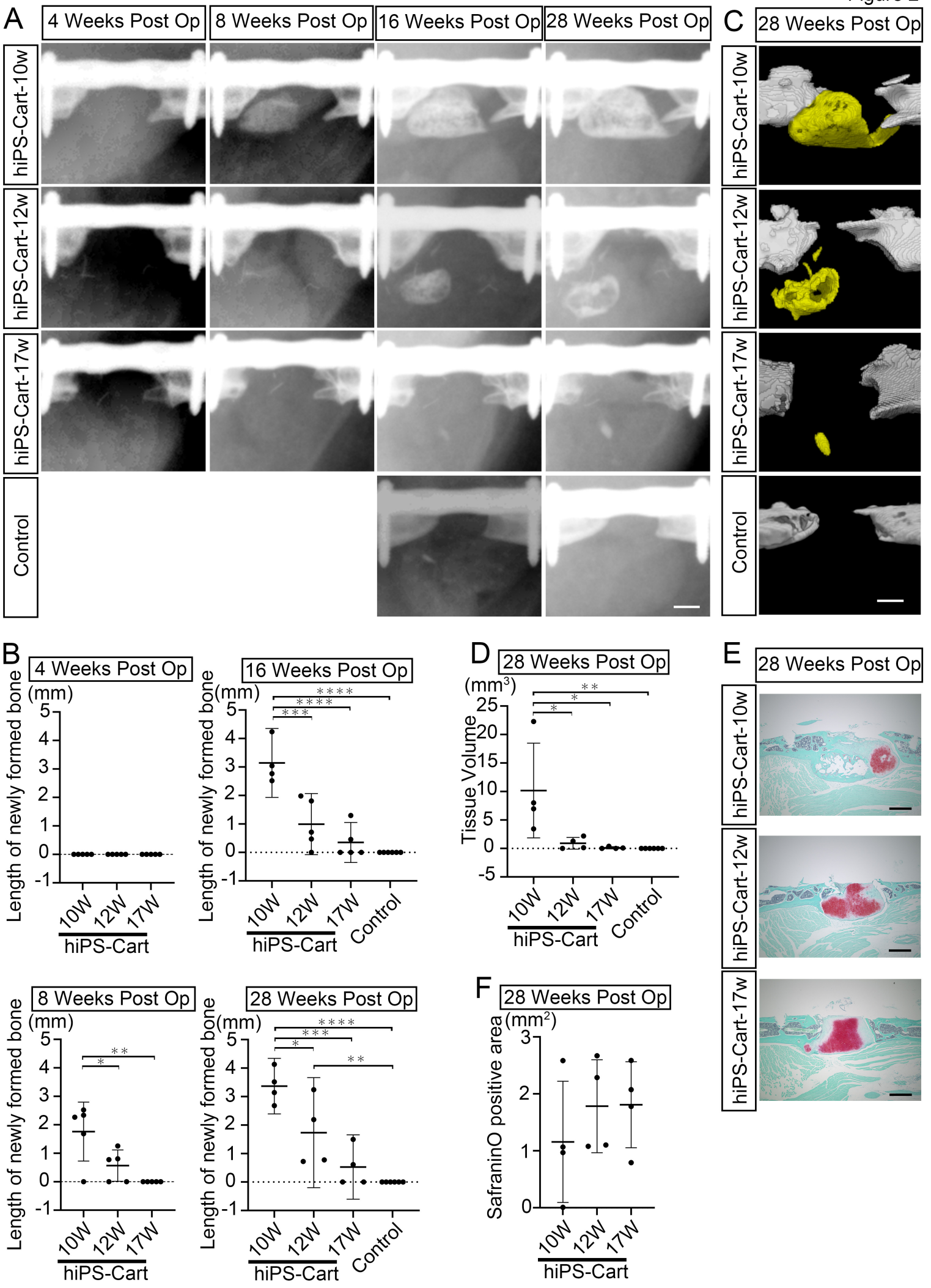
A
4 Weeks Post Op
8 Weeks Post Op
16 Weeks Post Op
28 Weeks Post Op
hiPS-Cart-10w
hiPS-Cart-12w
hiPS-Cart-17w
Control
C
28 Weeks Post Op
B
4 Weeks Post Op
16 Weeks Post Op
8 Weeks Post Op
28 Weeks Post Op
Length of newly formed bone (mm)
10W
12W
17W
Control
hiPS-Cart
D
28 Weeks Post Op
Tissue Volume (mm3)
E
28 Weeks Post Op
F
28 Weeks Post Op
SafraninO positive area (mm2)

Figure 3

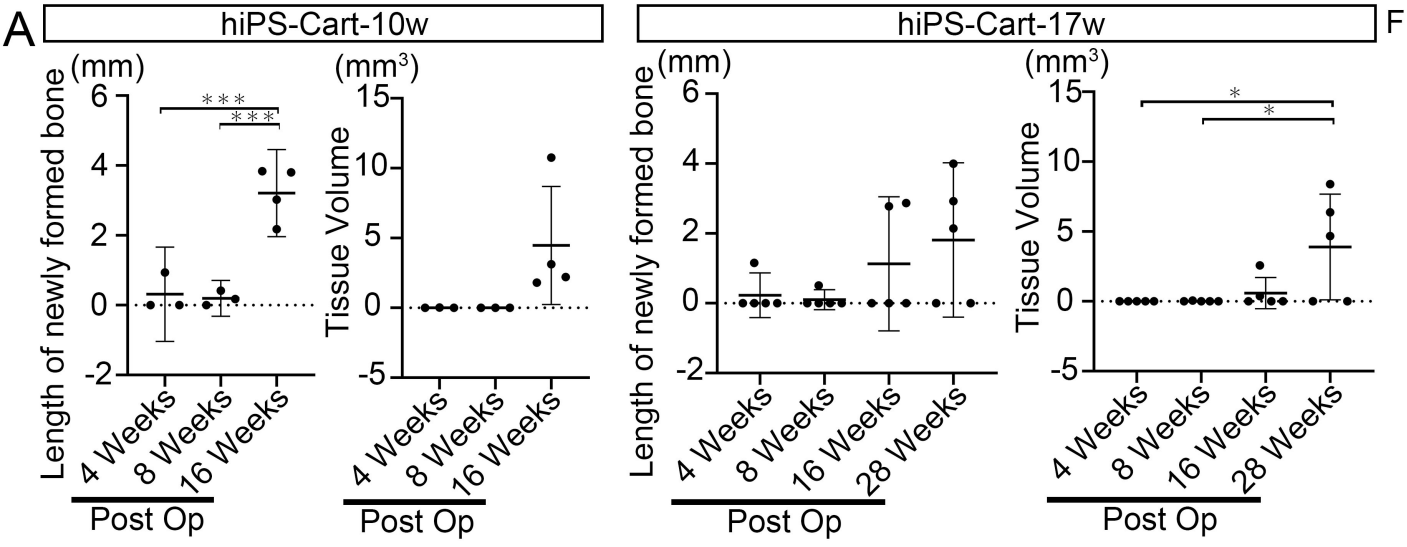
A
hiPS-Cart-10w
hiPS-Cart-17w
Length of newly formed bone
(mm)
Tissue Volume
(mm3)
***
***
*
*
4 Weeks
8 Weeks
16 Weeks
28 Weeks
Post Op

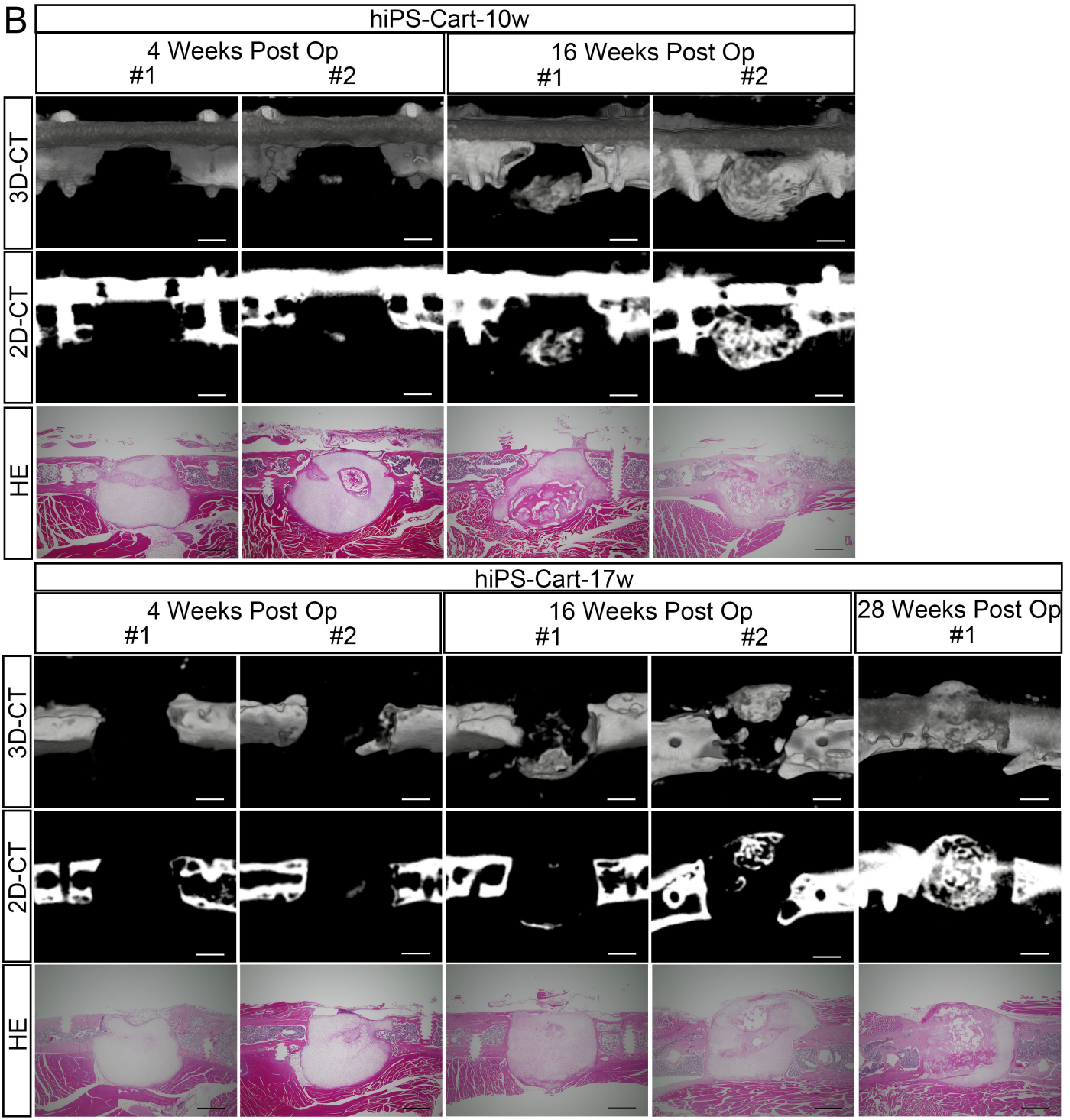
B
hiPS-Cart-10w
4 Weeks Post Op
16 Weeks Post Op
#1
#2
hiPS-Cart-17w
28 Weeks Post Op
3D-CT
2D-CT
HE

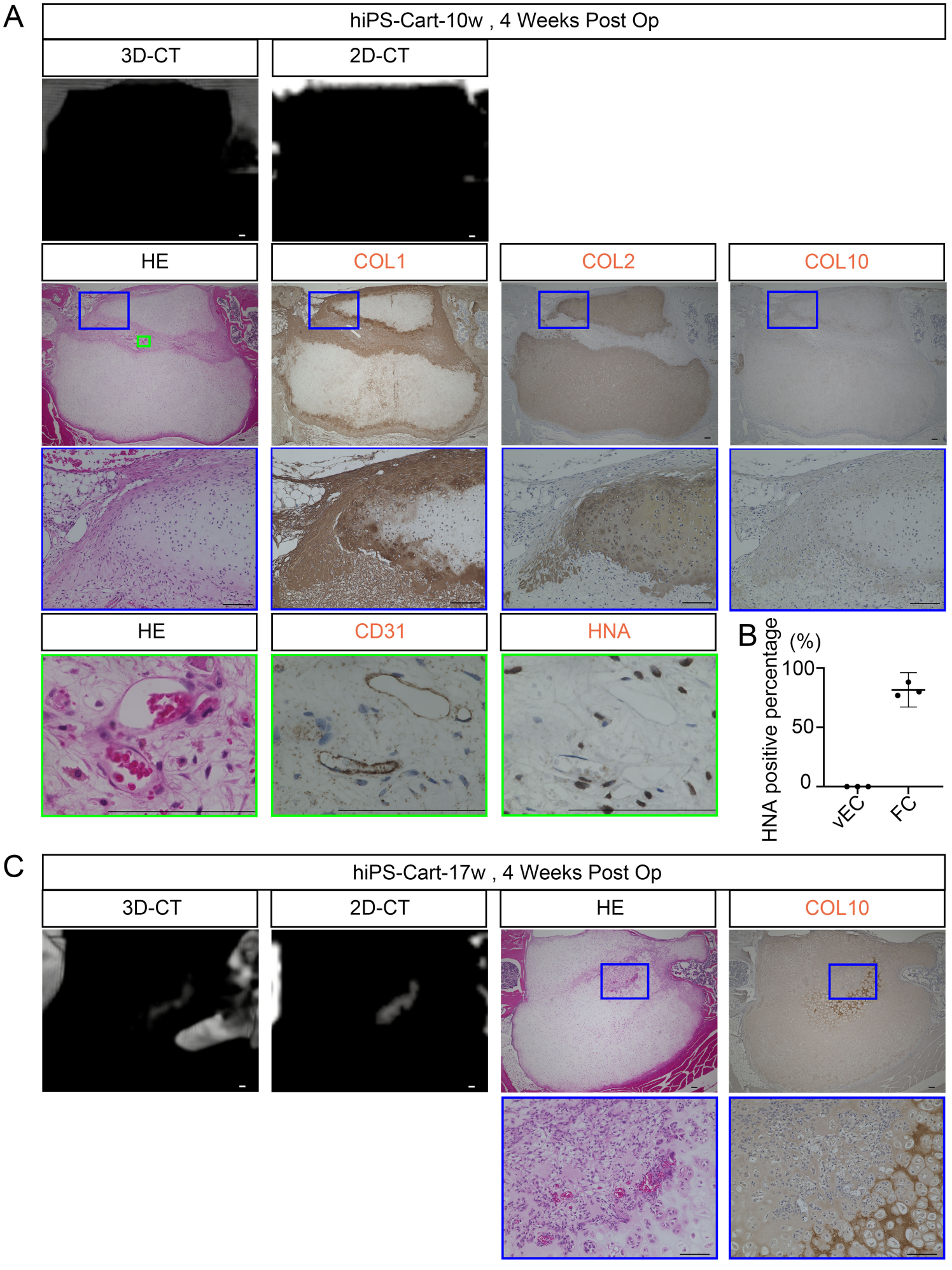
A
hiPS-Cart-10w , 4 Weeks Post Op
3D-CT
2D-CT
HE
COL1
COL2
COL10
HE
CD31
HNA
B
HNA positive percentage
(%)
100
50
0
vEC
FC
C
hiPS-Cart-17w , 4 Weeks Post Op
3D-CT
2D-CT
HE
COL10

A

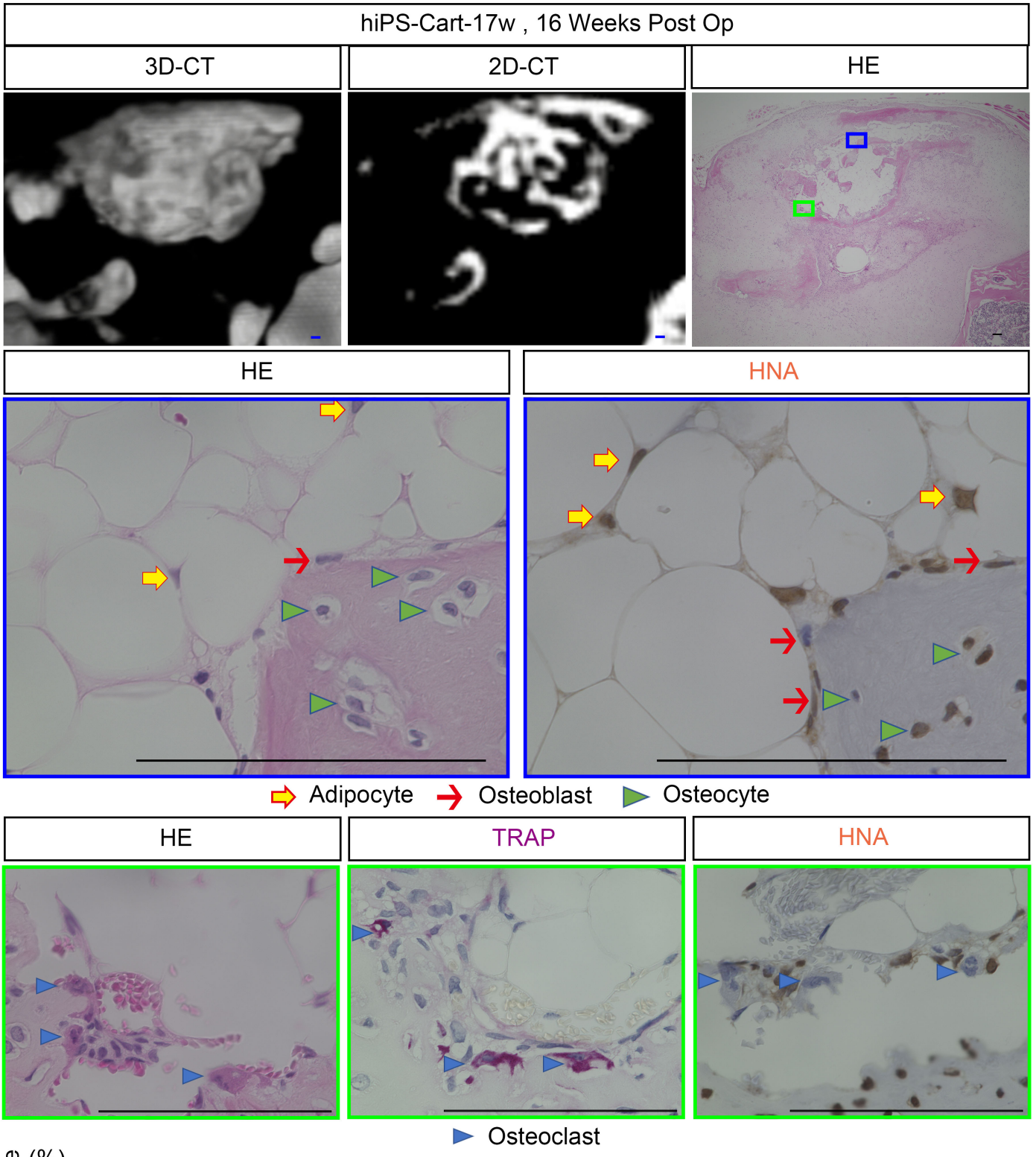
hiPS-Cart-17w , 16 Weeks Post Op
3D-CT
2D-CT
HE
HE
HNA
Adipocyte
Osteoblast
Osteocyte
HE
TRAP
HNA
Osteoclast

B

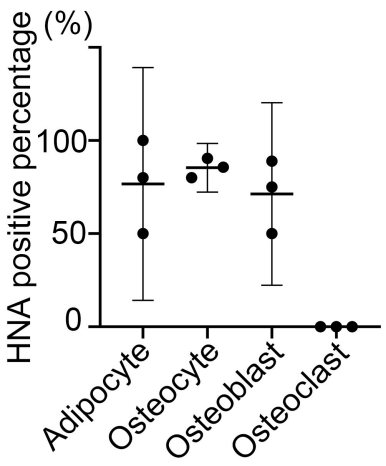
HNA positive percentage (%)
100
50
0
Adipocyte
Osteocyte
Osteoblast
Osteoclast

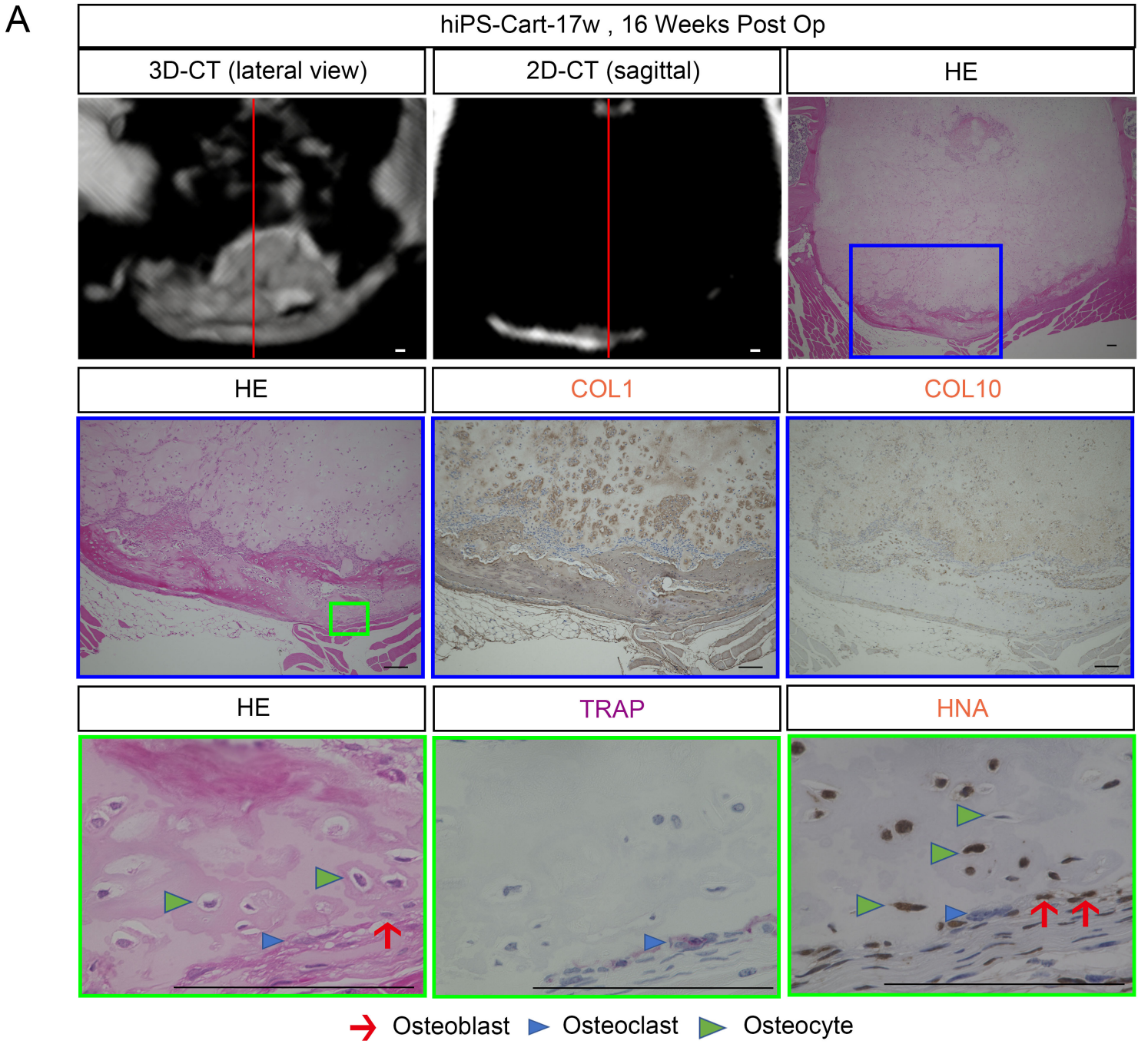
A
hiPS-Cart-17w , 16 Weeks Post Op
3D-CT (lateral view)
2D-CT (sagittal)
HE
HE
COL1
COL10
HE
TRAP
HNA
Osteoblast
Osteoclast
Osteocyte

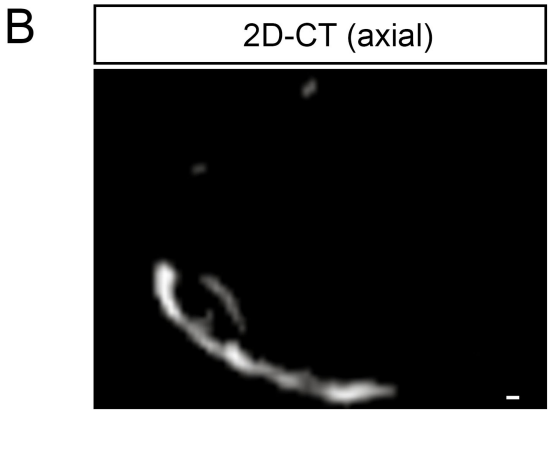
B
2D-CT (axial)

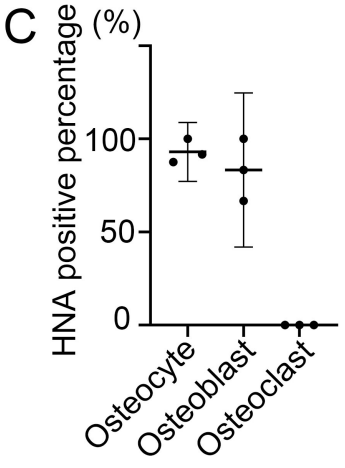
C
HNA positive percentage (%)
100
50
0
Osteocyte
Osteoblast
Osteoclast

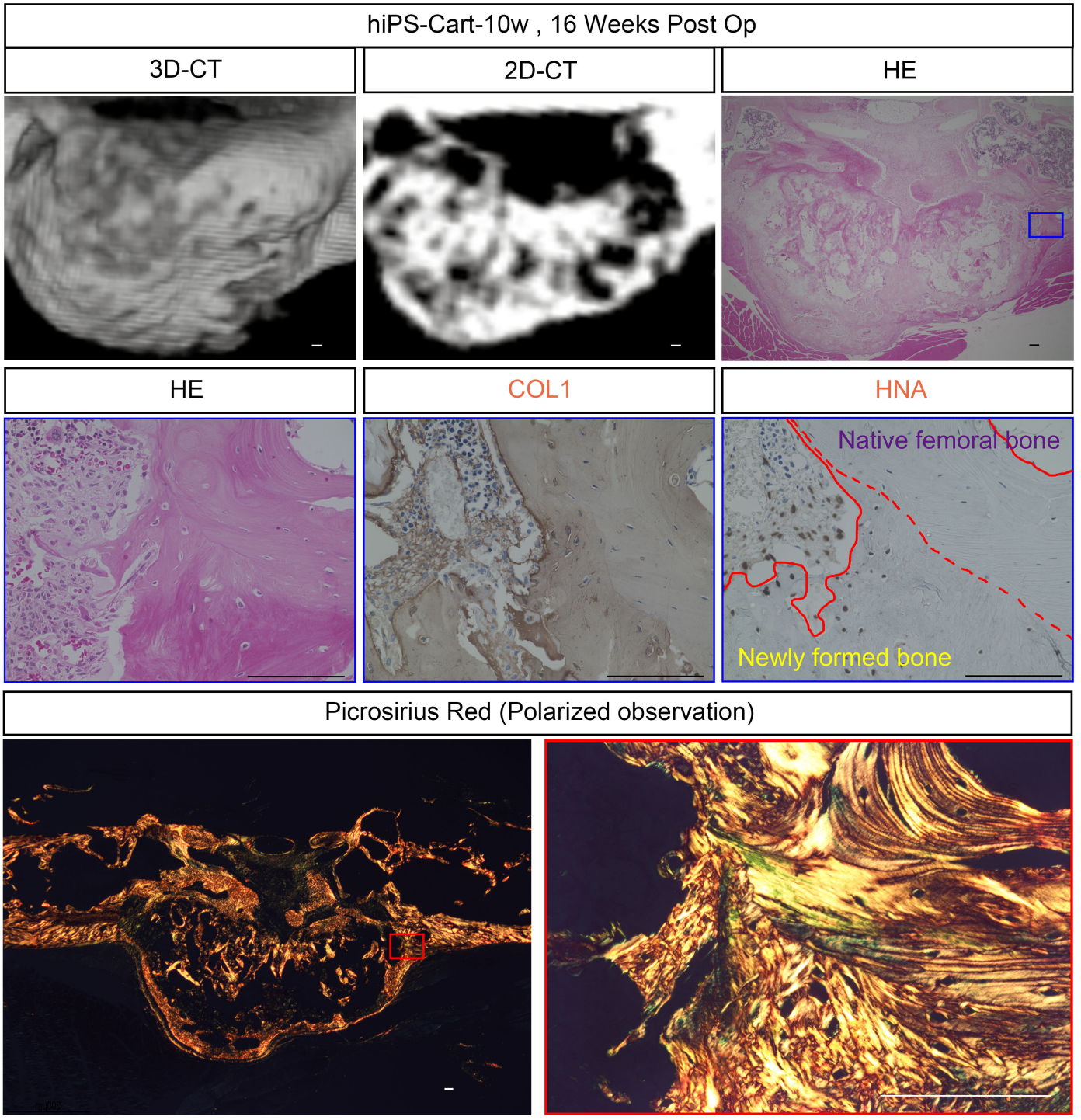
hiPS-Cart-10w , 16 Weeks Post Op
3D-CT
2D-CT
HE
HE
COL1
HNA
Native femoral bone
Newly formed bone
Picrosirius Red (Polarized observation)